The Journal of Physiology

Longitudinal and transversal propagation of excitation along the tubular system of rat fast-twitch muscle fibres studied by high speed confocal microscopy

Joshua N. Edwards[1], Tanya R. Cully[1], Thomas R. Shannon[2], D. George Stephenson[3] and Bradley S. Launikonis[1]

[1]*School of Biomedical Sciences, University of Queensland, Brisbane, Qld, Australia*
[2]*Department of Molecular Biophysics and Physiology, Rush University Medical Centre, Chicago, IL, USA*
[3]*Department of Zoology, La Trobe University, Melbourne, Vic, Australia*

Non-technical summary Contraction of the vertebrate skeletal muscle is dependent on the excitation of the highly specialized plasma membrane of individual muscle fibres. Most of the plasma membrane covers an extensive, structured network of narrow invaginating tubules, but little is known about how excitation propagates along the tubular network of mammalian skeletal muscle fibres in the radial and longitudinal directions with respect to the fibre axis. Here we show that excitation can take multiple pathways through the internal network of tubules in fast-twitch muscle fibres of the rat and determine the rates that excitation can spread within the internalized membrane tubules and show how this can change during muscle fatigue. Our results increase our understanding of mammalian skeletal muscle function in health, fatigue and some disease states.

Abstract Mammalian skeletal muscle fibres possess a tubular (t-) system that consists of regularly spaced transverse elements which are also connected in the longitudinal direction. This tubular network provides a pathway for the propagation of action potentials (APs) both radially and longitudinally within the fibre, but little is known about the actual radial and longitudinal AP conduction velocities along the tubular network in mammalian skeletal muscle fibres. The aim of this study was to track AP propagation within the t-system network of fast-twitch rat muscle fibres with high spatio-temporal resolution when the t-system was isolated from the surface membrane. For this we used high speed confocal imaging of AP-induced Ca^{2+} release in contraction-suppressed mechanically skinned fast-twitch fibres where the t-system can be electrically excited in the absence of the surface membrane. Supramaximal field pulses normally elicited a synchronous AP-induced release of Ca^{2+} along one side of the fibre axis which propagated uniformly across the fibre. In some cases up to 80 or more adjacent transverse tubules failed to be excited by the field pulse, while adjacent areas responded with normal Ca^{2+} release. In these cases a continuous front of Ca^{2+} release with an angle to the scanning line was observed due to APs propagating longitudinally. From these observations the radial/transversal and longitudinal AP conduction velocities along the tubular network deeper in the fibre under our conditions ($19 \pm 1^{\circ}C$) ranged between 8 and 11 $\mu m\ ms^{-1}$ and 5 to 9 $\mu m\ ms^{-1}$, respectively, using different methods of estimation. The longitudinal propagation of APs appeared to be markedly faster closer to the edge of the fibre, in agreement with the presence of dense longitudinal connections immediately below the surface of the fibre and more sparse connections at deeper planes within the fibre. During long trains of closely spaced field pulses the AP-elicited Ca^{2+} releases became non-synchronous along the fibre axis. This is most likely caused by local tubular K^+ accumulation that produces local depolarization and local slowing of AP propagation. Longitudinally propagating APs may reduce such inhomogeneities by exciting areas of delayed

DOI: 10.1113/jphysiol.2011.221796

AP onset. Clearly, the longitudinal tubular pathways within the fibre for excitation are used as a safety mechanism in situations where a local depolarization obstructs immediate excitation from the sarcolemma. Results obtained from this study also provide an explanation for the pattern of contractures observed in rippling muscle disease.

(Received 3 October 2011; accepted after revision 6 December 2011; first published online 12 December 2011)
Corresponding author B. S. Launikonis: School of Biomedical Sciences, University of Queensland, Brisbane, Qld, 4072, Australia. Email: b.launikonis@uq.edu.au

Introduction

Skeletal muscle is a large organ consisting of specialized fibres that are highly elongated and have large diameters. For normal function, the muscle must respond rapidly to surface membrane excitation with a uniform release of Ca^{2+} in the order of milliseconds. Skeletal muscle has adapted in a number of ways to minimize time delays between excitation at the neuromuscular junction, Ca^{2+} release and contraction (Julian *et al.* 1986; Young & Rome, 2001; Rome, 2006; Stephenson, 2006). A major specialization of muscle fibres to achieve a rapid response to stimulation was the development of a tubular network known as the tubular (t-) system which is in connection with the extracellular space and in continuation with the surface membrane, or sarcolemma. The t-system membrane system is largely made up of (i) transverse tubules that wrap around each myofibril, (ii) a sub-sarcolemmal network that joins the sarcolemma to the transverse tubules, and (iii) intermittent longitudinal tubules seemingly at all planes inside the fibre that link up adjacent transverse tubules (Veratti, 1961). The transverse tubules house the voltage sensors for excitation–contraction (EC) coupling and are aligned in close apposition to the terminal cisternae of the internal Ca^{2+} store, the sarcoplasmic reticulum or SR. These junctional membranes meet at every sarcomere throughout the muscle fibre for the purpose of initiating rapid, uniform Ca^{2+} release in response to action potential (AP) stimulation, leading to contraction of the fibre.

Excitation in the form of APs generated at the neuromuscular junction should reach the mouths of the transverse tubules (the junctions with the sarcolemma) uniformly in mammalian muscle fibres due to the rapid propagation of APs along the sarcolemma (e.g. $1\ m\ s^{-1}$ or faster in fast-twitch rat muscle at 22°C; Kössler *et al.* 1991). APs should then propagate along all transverse tubules. Because of the large difference in diameter of the transverse tubules compared to that of the fibre one would expect that the radial propagation rate of action potentials inside fast-twitch fibres is considerably slower than is the case across the sarcolemma (Hodgkin, 1954). Estimates of the radial propagation velocity of APs in frog muscle fibres fall between 25 and 75 $\mu m\ ms^{-1}$ (20–25°C) (Adrian *et al.* 1969; Gonzalez-Serratos, 1971; Nakajima & Gilai, 1980). However, no such measurements have been made in mammalian skeletal muscle fibres where the structure of the t-system is very different from that in skeletal muscle fibres of anurans (Eisenberg, 1983). The fractional volume of the t-system is similar in rat and toad skeletal muscle fibres (Launikonis & Stephenson, 2002*a*) but the volume-to-surface area is considerably larger in toad than in rat skeletal muscle (Hodgkin & Nakajima, 1972; Adrian & Peres, 1979; Dulhunty, 1984; Launikonis & Stephenson, 2002*a*). Therefore the AP conduction velocity in the tubular system of mammalian fast-twitch muscle should be slower than that in anuran muscle if other membrane properties were the same.

An interesting observation was made by Posterino *et al.* (2000) who showed that APs could propagate longitudinally through the t-system of skeletal muscle fibres. This conclusion was based on recordings of spontaneously propagating contractures through mechanically skinned fibres at temperatures >26°C that were sensitive to tetrodotoxin, Na^+ and K^+ gradients and perturbations to the t-system. The complexity of the longitudinal elements of the t-system and propagation of APs in this direction must have important functional implications for muscle function in health, disease and fatigue. However fundamental knowledge of AP propagation properties in longitudinal and transversal directions with respect to the fibre axis of mammalian skeletal muscle fibres to ensure the uniform release of Ca^{2+} during EC coupling is currently lacking.

To examine the role of transversally and longitudinally propagating APs we imaged: (i) AP-induced Ca^{2+} release in mechanically skinned fibres from rat muscle using a high-speed laser scanning confocal microscope; and (ii) the t-system at different planes in the fibre. Skinned fibres allowed the examination of t-system structure and properties in the absence of a sarcolemma without affecting EC coupling (Posterino *et al.* 2000; Launikonis & Stephenson, 2002*b*, 2004; Launikonis *et al.* 2006). Field stimulation provided uniform depolarization of the sealed t-system on one side of the fibre and the presence of APs was visualised from the front of Ca^{2+} release imaged at microsecond resolution. Here we measure for the first time the radial and longitudinal AP conduction velocities in mammalian fast-twitch fibres and show that longitudinal propagation of action potentials ensures a uniform release of Ca^{2+} during EC coupling. These results have implications for our fundamental understanding of EC coupling in health and some disease states.

Methods

The authors have read, and the experiments comply with the policies and regulations of The Journal of Physiology given by Drummond (2009). All experimental methods were approved by the Animal Ethics Committee at The University of Queensland. Fifteen male Wistar rats (250–300 g) were killed by CO_2 asphyxiation and the extensor digitorum longus (EDL) muscles were rapidly excised. Muscles were then placed in a Petri dish under paraffin oil above a layer of Sylgard. Individual fibres were then isolated and mechanically skinned. Skinned fibres were transferred to a custom built experimental chamber with a coverslip bottom, where they were bathed in a standard K^+-repriming solution, where the sealed t-system becomes polarized to physiological levels (Ørtenblad & Stephenson, 2003; Stephenson, 2006). The preparation was positioned in the chamber between two platinum electrodes, which ran parallel to the long axis of the mounted fibre. Skinned fibres were electrically stimulated with a field pulse of 50–70 V cm^{-1} for 1 or 2 ms, as described previously (Posterino *et al.* 2000; Launikonis *et al.* 2006). To image Ca^{2+} inside the t-system skinned fibres were prepared as described previously (Launikonis & Stephenson, 2002*b*). Briefly, intact fibre bundles were isolated from EDL muscles whilst under paraffin oil and they were flushed with a physiological solution containing 1 mM fluo-5N for about 1 min. This solution was left on the bundle of fibres for more than 10 min to allow it to diffuse throughout the bundle and into the t-system. Individual fibres were then isolated and mechanically skinned. Skinned fibres were transferred to an experimental chamber that used a coverslip as a base under a droplet of Na^+-based Ca^{2+} loading solution.

The standard K^+-repriming solution contained (mM): K^+, 126; Na^+, 36, Mg^{2+}, 1; HDTA, 50; Hepes, 90; EGTA, 0.01; ATP, 8; CP, 10; and Oregon Green Bapta 5N (OGB5N), 0.05. [Ca^{2+}] was expected to be between 80–100 nM (Lamb & Stephenson, 1990; Posterino *et al.* 2000). In some experiments OGB5N was replaced with rhod-2. Osmolality was adjusted to 290 ± 10 mosmol kg^{-1} with sucrose and pH was set to 7.10 with KOH. This solution kept the sealed t-system polarized (Lamb & Stephenson, 1994). *n*-Benzyl-*p*-toluene sulphonamide (BTS; Sigma-Aldrich Co., St Louis, MO, USA; 50 μM) was added to suppress contraction without affecting excitability or Ca^{2+} movements (Cheung *et al.* 2002; Macdonald *et al.* 2005). The Na^+-based Ca^{2+}-loading solution had similar components to the standard internal solution except that all K^+ was replaced with Na^+, EGTA was raised to 1 mM and [Ca^{2+}] was set at 800 nM.

Ca^{2+}-dependent fluorescence of rhod-2 and OGB5N was imaged using a Zeiss 5 LIVE confocal microscope (Carl Zeiss MicroImaging GmbH, Germany) with a slit scanner for high speed scanning focused onto the preparation through a 40× water immersion lens. Imaging was in *xt* and *xyt* mode with the laser scanning at 15.5 and 25 μs line^{-1}, respectively. The scanning line was positioned parallel to the long axis of the fibre to capture the rise of AP-induced Ca^{2+} release across the maximum number of sarcomeres. OGB5N and rhod-2 were excited at 488 and 543 nm from Ar ion and HeNe lasers, respectively. The t-system with trapped fluo-5N was imaged with a FV1000 confocal laser-scanning microscope (Olympus, Tokyo, Japan) using a water immersion objective (60×, NA 1.0) and the 488 nm line of a multi-line Ar ion laser. Linescanning of cytoplasmic rhod-2 fluorescence during AP-induced Ca^{2+} release was also performed on this confocal microscope at 2.1 ms line^{-1}.

The data are presented as means ± SEM. All experiments were carried out at 19 ± 1°C to avoid excessive damage to our preparations due to increased reactive oxygen species production at 37°C (Edwards *et al.* 2007) and to increase the temporal resolution of our experiments.

Results

A uniform and rapid excitation of the t-system along the long axis in mechanically skinned fibres

The sarcolemma coordinates the movement of APs on the fibre surface and the propagation into the transverse tubules via the subsarcolemmal tubular network. To answer the question of whether the t-system network ensures uniform excitation within the fibre and to track the propagation rate of APs through the t-system, we have used skinned fibres where the sarcolemma has been removed to allow isolation of the t-system. We have previously shown that the t-system in mechanically skinned fibres (i) seals off (Launikonis & Stephenson, 2002*b*, 2004), (ii) becomes normally polarized when bathed in the K^+-based solution mimicking the internal environment described in Methods (K^+-repriming solution) (Lamb & Stephenson, 1994), and (iii) is excitable (Posterino *et al.* 2000). Using procedures that interfere with the generation and propagation of APs we also showed that the force responses (and implicitly the associated Ca^{2+} transients) elicited in mechanically skinned fibres by electrical stimuli, as well as the spontaneous large force responses (and implicitly the associated Ca^{2+} transients) are the result of propagated APs generated in the sealed t-system (see e.g. Posterino *et al.* 2000; Ørtenblad & Stephenson, 2003; Stephenson, 2006).

To measure the excitability of the t-system with high spatio-temporal resolution, the AP-induced release of Ca^{2+} was imaged at scanning rates in the microsecond range (15.5 μs line^{-1}) when contraction was suppressed with BTS (see Methods). Changes in

cytoplasmic [Ca^{2+}] were faithfully followed using a fast-reacting ($k_{off} = 5.6\ ms^{-1}$), low affinity Ca^{2+}-sensitive dye ($k_D = 32.9\ \mu M$), OGB5N (Quiñonez *et al.* 2010). This allowed the tracking of the AP pathways within the t-system network with minimal delay. Figure 1 shows an image of the fluorescence signal emitted by cytoplasmic OGB5N in a skinned fibre during supramaximal field stimulation at 2 Hz. The slit scanning laser was focused in the middle of the fibre, parallel to its long axis and the field stimulation protocol is shown at top of Fig. 1*A*. In the image of Fig. 1*A*, the succession of AP-elicited Ca^{2+} transients is shown in a compressed form, effectively at the temporal resolution of a 'conventional' scanning confocal microscope. The spatially averaged fluorescence profile is shown immediately below (Fig. 1*B*).

Figure 1*C–E* shows each of the rising phases of the transients in Fig. 1*A* with an expanded time axis and Fig. 1*F* displays the spatially averaged profiles. Properties of these transients are noted in the figure legend. An inspection of the fronts of Ca^{2+} release in Fig. 1*C–E* reveals only minor inhomogeneities in the order of less than hundreds of microseconds in the rise of the Ca^{2+} transient across more than 100 μm of fibre. The rise time (RT) of the transient marked '*c*' was 1.10 ms (Fig. 1). The average RT of the first Ca^{2+} transient from four fibres that responded in similar uniform fashion as in Fig. 1 was 1.21 ± 0.16 ms. This is very similar to the RT recorded with a fast reacting, low affinity Ca^{2+} dye (mag-fluo-4) in intact, enzymatically isolated EDL fibres from mouse at 22°C (1.15 ± 0.04 ms) using high acquisition rate

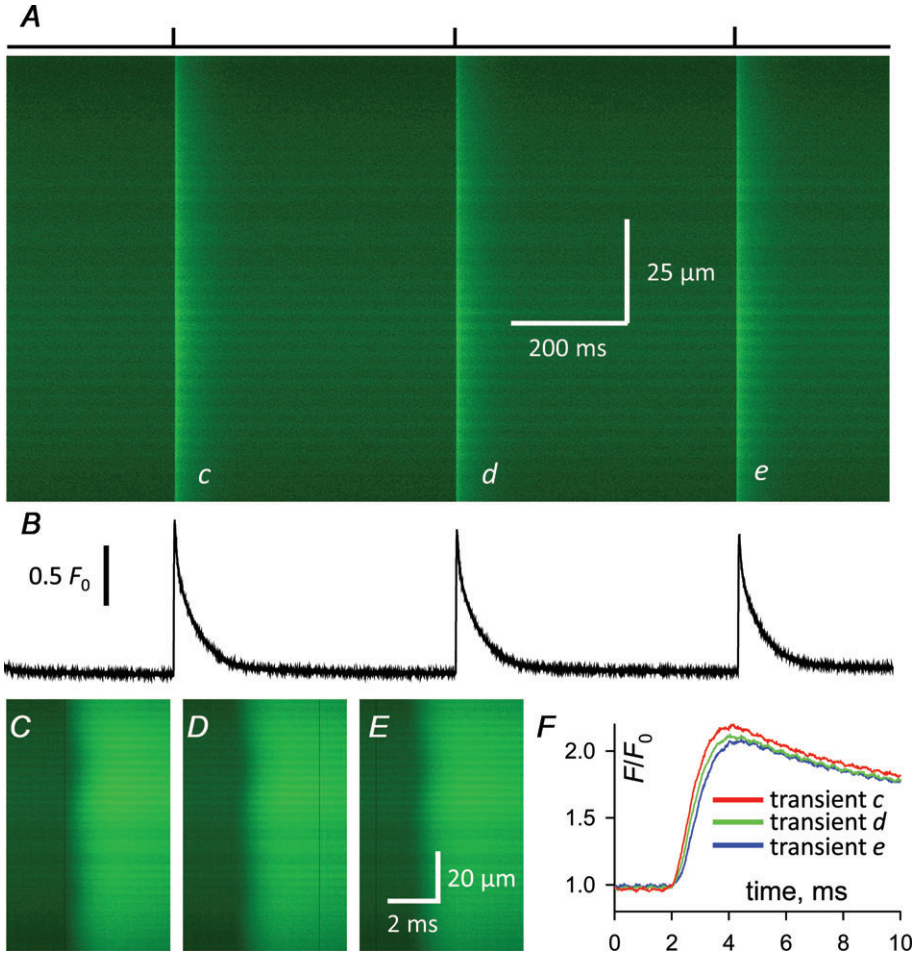

Figure 1. High speed confocal imaging of cytoplasmic Ca^{2+} shows that AP-induced Ca^{2+} release is very uniform along the length of the skeletal muscle fibres
A, linescan image of OGB5N fluorescence from the cytoplasm of a skinned fast-twitch rat EDL fibre in an area close to the longitudinal axis of the fibre during field stimulation at 2 Hz. The stimulation protocol is indicated at the top of the image and the spatially averaged profile is presented below in *B*. Each Ca^{2+} transient is marked with a lower-case letter in *A* and is displayed on an expanded time axis in the panel with the corresponding upper-case letter, *C–E*. Note that the foot of the Ca^{2+} transient is almost completely synchronous across more than 100 μm in all three cases. *F*, the spatially averaged transients with an expanded time axis. The amplitude and 10–90% rise time for each transient were, respectively: 1.17 and 1.10 ms (c); 1.11 and 0.80 ms (*d*); and 1.08 and 0.98 ms (*e*).

photometry (Calderón *et al.* 2010). This shows that the degree of spatial inhomogeneities imaged during AP-induced Ca^{2+} release in skinned fibres (Fig. 1) cannot be greater than in the intact fibres, since otherwise the RT would be much longer. Transients *d* and *e* differed only slightly from transient *c* (Fig. 1).

Propagation of excitation along the short and long axis of the t-system

In Fig. 2 the slit scanning laser was focused in the middle of the fibre, but at a slight angle to the long fibre axis and the image of the fluorescence signal emitted by cytoplasmic OGB5N is shown during two spontaneously elicited APs (Ca^{2+} transients marked *c* and *e*), and in response to two supramaximal field stimuli indicated at top of Fig. 2*A* (Ca^{2+} transients marked *d* and *f*). The fronts of the Ca^{2+} transients elicited by the first spontaneous AP and the first externally applied stimulus are shown at high temporal resolution in Fig. 2*C* and *D*, respectively. APs triggered by the external pulses are generated in the closed t-tubules on the side of the fibre closest to the cathode and then propagate transversally across the short axis of the fibre (Stephenson, 2006). The slight angle between the Ca^{2+} release front elicited by electrical stimulation in Fig. 2*D* and the scanning line shows that the Ca^{2+} release front and implicitly the stimulus-induced AP propagate transversally across the short axis of the fibre. The middle and the bottom traces in the right hand side panel labeled 'transversal' in Fig. 2*E* are fluorescence profiles of the two regions indicated by the black bars at the left of Fig. 2*D*. The small delay in the rise of the fluorescence signal in the bottom right hand side trace compared to that in the middle right hand side trace shows that the transversal front of the Ca^{2+} transient propagates left to right. The velocity of propagation of the Ca^{2+} release front in a direction perpendicular to it and across the short axis of the fibre was close to 9.5 μm ms^{-1}.

The spontaneous Ca^{2+} transient marked *c* in Fig. 2*A* displayed a front at a different angle from the scanning line in Fig. 2*C*, indicative of propagation at constant velocity along the direction of the scanning line, which is almost parallel to the long axis of the fibre. The middle and the bottom traces in the left hand side panel labeled 'longitudinal' in Fig. 2*E* are fluorescence profiles of the two regions indicated by the left black bars at the middle and the bottom parts of Fig. 2*C*. Note that the black bars at the left of Fig. 2*C* and *D* correspond to the same physical location on the fibre. The fluorescence signal rises with a delay of about 7.5 ms in the middle left hand side trace compared with that at the bottom left hand side trace, indicating that the Ca^{2+} transient propagates upwardly along the long axis of the fibre. Since the distance between the two locations along the long fibre axis corresponding to the two black lines in Fig. 2*C* is about 44 μm, it follows that the velocity of the Ca^{2+} transient and implicitly of the AP propagation in the longitudinal direction is close to 6.3 μm ms^{-1} (44 μm/7 ms). A more accurate way to measure the propagation velocity along the scanning line is directly from the tangent of the angle made by the Ca^{2+-} front with the *x*-axis. From Fig. 2*C*, the longitudinal propagation velocity in this example was 6.8 μm ms^{-1} which in this particular case was about 25% lower than the velocity of the Ca^{2+} release front propagating transversally across the fibre at the same location. This velocity is similar to the rate of longitudinal propagation of APs previously reported in skinned fibres from force measurements (adjusted for recording at a higher temperature with a Q_{10} of 2; Posterino *et al.* 2000) and suggests this is the same phenomenon. These spontaneous events can be observed originating from a point to propagate longitudinally (see online Supplemental Material, Fig S1). We observed such spontaneous, propagating releases of Ca^{2+} in 17 of 46 fibres imaged on either a conventional or a high-speed scanning confocal microscope. Their average propagation rate was 7.9 ± 0.4 μm ms^{-1} ($n = 17$). The observed propagating release front cannot be due to Ca^{2+}-induced Ca^{2+} release (CICR; Endo *et al.* 1970; Ford & Podolsky, 1970) because this mechanism is absent from mammalian skeletal muscle and otherwise the velocity of CICR propagation is one to two orders of magnitude slower that the velocity of propagation of the Ca^{2+} release front (Fig. 2; Shirokova *et al.* 1996; Launikonis & Stephenson, 2000; Zhou *et al.* 2005).

Thus the Ca^{2+} transients elicited by field pulses (*d* and *f*) and those observed spontaneously (*c* and *e*) are the result of transversally and longitudinally propagating APs, respectively. We can provide strong further evidence that this is the case if the RT and amplitude of the Ca^{2+} transient in a narrow specific region of the fibre is not dependent on the direction from which the AP arrives at that point. This is because the same amount of Ca^{2+} is locally released during the very brief opening of the sarcoplasmic reticulum Ca^{2+} release channels during an AP (Baylor & Hollingworth, 2003; Posterino & Lamb, 2003). Figure 2*E* shows a series of spatially averaged profiles derived from regions of the images of Fig. 2*C* and *D*. The top two profiles in Fig. 2*E* are the averaged profiles along the entire region of space displayed in Fig. 2*C* and *D* that represent APs predominantly moving longitudinally and transversally, respectively. As expected, when averaged over a large area (across 100 μm) the longitudinally propagating APs induce a slowly rising Ca^{2+} transient whereas the field pulse-elicited transversally propagating APs induce a fast rising transient. However, when the spatially averaged profile is restricted to the same narrow region of space along the fibre (about 5 μm or two to three sarcomeres) the Ca^{2+} transients look very similar (Fig. 2*E*, middle two and lower two profiles). We can compare this quantitatively

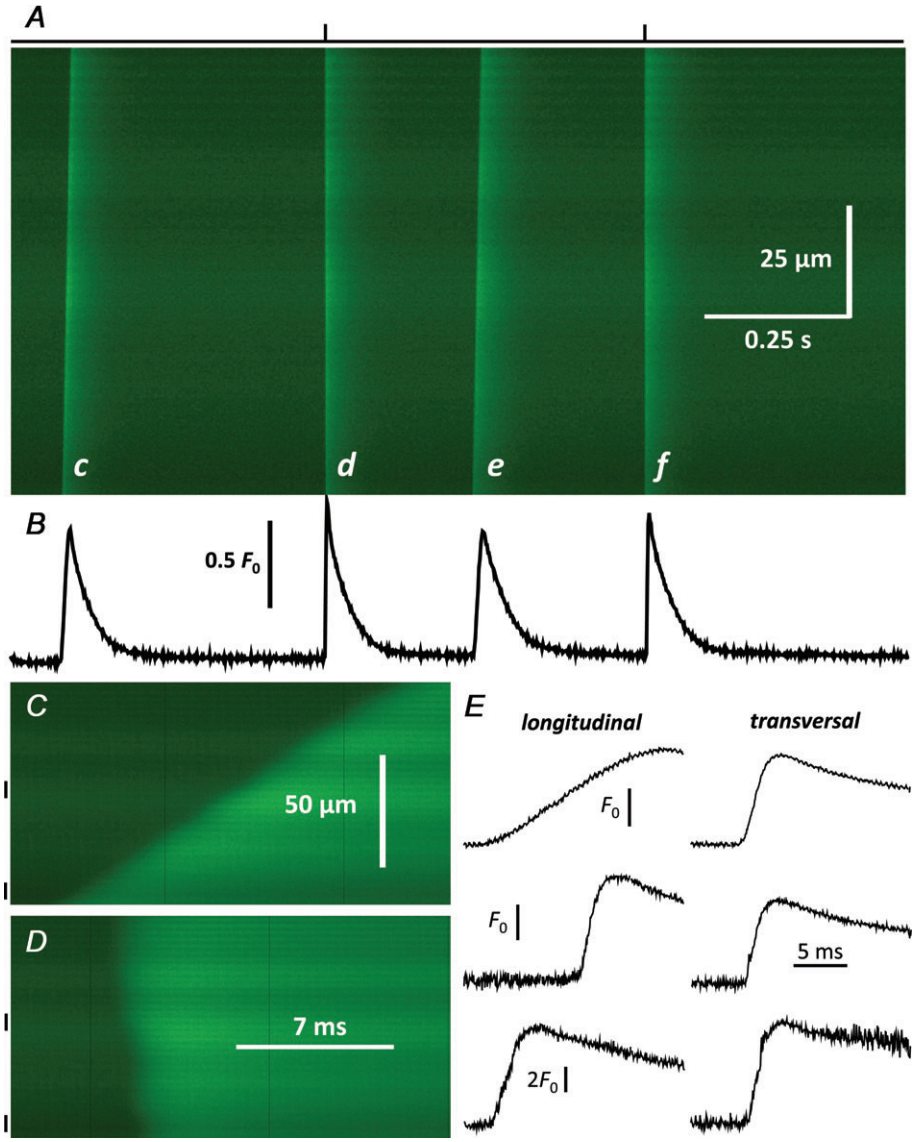

Figure 2. Longitudinally and transversally propagating APs activate Ca^{2+} release in the same fashion
A, linescan image of OGB5N fluorescence from the cytoplasm of a rat skinned fibre during field stimulation. The fibre was electrically stimulated twice as indicated by the bar at the top of *A*. Field pulses resulted in Ca^{2+} transients that had a release front at a small angle with respect to the scanning line, marked *d* and *f*. Two other Ca^{2+} transients, marked *c* and *e*, were spontaneously elicited during this linescan. Note that the release fronts of these Ca^{2+} transients were tilted to the right compared with the release fronts of the Ca^{2+} transients triggered by electrical stimulation. *B*, spatially averaged profile of the linescan. *C* and *D*, the Ca^{2+} transients marked with lower-case letters *c* and *d* in A are displayed on an expanded time axis in the panels with the corresponding upper-case letters. Note that the Ca^{2+} release front in *C* is continuous with a constant angle to the scanning line, showing that the Ca^{2+} transient and implicitly the AP propagated over a long distance within the fibre. The velocity of propagation in the direction of movement (left to right) of the scanning line, which is almost parallel with the long axis of the fibre, can be calculated from the tangent of the angle formed by the Ca^{2+} release front with the *x*-axis, in this case is 6.8 μm ms^{-1}. In *D* the field pulse induced a Ca^{2+} release front that was on a slight angle to the scanning line, because the line was not completely parallel to the long axis of the fibre. The velocity of propagation of the Ca^{2+} transient and underlying AP in transversal direction, perpendicular on the Ca^{2+} release front is calculated at 9.5 μm ms^{-1}. In *E* spatially averaged profiles from *C* ('longitudinal') and *D* ('transversal') that represent the two directions of AP propagation within the t-system are presented. The top traces are averaged profiles across the entire length of space in *C* and *D*, respectively. The remaining traces are profiles from the spatially restricted regions indicted by the black bars at the left of the images in *C* and *D*. The traces in the middle row of *E* are the profiles from the regions indicted by the left bars at the middle of the images in *C* and *D*, respectively. The bottom two traces in *E* are the profiles from the regions indicated by the lower left

by determining the ratio of the RT of the Ca^{2+} transients and also the amplitudes of the signals elicited by APs reaching the same narrowly defined region of space when APs propagate transversally *vs.* longitudinally. If subscripts 'T' and 'L' refer to transversal and longitudinal propagation of APs, respectively and 'Amp' refers to the amplitude of the Ca^{2+} transient in the narrowly restricted space, from three preparations RT_T/RT_L and Amp_T/Amp_L were 0.97 ± 0.27 and 0.91 ± 0.07, respectively. As neither of the two results was different from 1 ($P > 0.1$, *t* test), this further supports the view that the Ca^{2+}-transients recorded in this study are caused by propagating APs.

Next, we will show that a combination of radially and longitudinally propagating APs can produce a Ca^{2+} transient that has a continuous front along the fibre axis even when inhomogeneities were initially present. Figure 3 is an image of AP-induced Ca^{2+} release of a fibre excited at 5 Hz and recorded in the same fashion as that shown in Fig. 1. In this instance not all tubules along the long axis of the fibre were synchronously excited during stimulation, as judged from the front of the first Ca^{2+} transient (marked '*c*'), which is not completely uniform. The linescan swept a region of the fibre centrally located. The transients that follow appear more uniform. Figure 3*C–J* shows the individual Ca^{2+} transients from Fig. 3*A* of corresponding lower-case letter displayed on an expanded time axis. Transient *c* did not have a uniform front with the scanning line. This transient started in two regions along the imaged section of the fibre and then propagated into the areas that did not initially release Ca^{2+}. The front of Ca^{2+} release across more than 100 μm was continuous and moved along the long axis of the fibre at 8.0 ± 0.6 μm ms^{-1} ($n = 5$ fibres, where the linescan swept a region of the fibre located at least 10 μm from the fibre surface) to the initially not excited areas. The '>' shape of the front of Ca^{2+} release was symmetrical in this example and in all four other fibres imaged in this way during field stimulation where this phenomenon occurred. This suggests that APs propagate into the areas that fail to respond to surface excitation from opposite adjacent areas along the long axis of the fibre at the same velocity.

The largest area that failed to be excited in the experiment shown in Fig. 3 by the field pulse was 40 μm (indicated by the arrow on Fig. 3*C*). During the subsequent stimulations the Ca^{2+} transients were more uniform in response to field stimulation, showing that the initial electrical stimulus was not strong enough to excite uniformly the tubular system along the entire length of the fibre and that the excitability of that particular area increased following excitation from longitudinally located adjacent segments of the tubular system (Fig. 3*C–F*). In this train of responses, the RT was briefest and the amplitude of the transient was maximal in transient *f*, where the front of the Ca^{2+} transient had become more uniform than the preceding transients implying that the tubular elements along the fibre axis became more synchronously excited.

We can look for inhomogeneities of excitation of transverse tubules from surface excitation under conditions that more closely mimic a physiological situation by applying long trains of closely spaced pulses to a fibre. During such frequently repeated stimuli, skeletal muscle responds with a prolonged force response. However this mode of stimulation can also lead to accumulation of K^+ in the small t-system lumen and depolarization. This causes fading of the force response, a phenomenon known as fast onset or high frequency fatigue (Allen *et al.* 2008; Cairns & Lindinger, 2008). Fading is probably due to a global depolarization of the t-system causing changes in the AP waveform, refractoriness or both. Preceding this, one would expect that local episodes of high frequency fatigue should present before a more global depolarization of the t-system occurred. Such events have not been reported before. In our experiments we could expect to observe a local delay in AP-induced Ca^{2+} release to develop following initial transients in the train that were uniform in their spatio-temporal release of Ca^{2+} in response to field stimulation.

Figure 4*A* shows AP-induced Ca^{2+} release in a skinned fibre stimulated at 10 Hz for more than 1.5 s under conditions of suprathreshold field pulse stimulation. Note that the internal bathing solution of the skinned fibre did not contain Cl^- and was therefore expected to more rapidly accumulate K^+ in the t-system during a train of action potentials than in the presence of a repolarizing tubular Cl^- current (Dulhunty, 1979; Dulhunty *et al.* 1986; Dutka *et al.* 2008; Fraser *et al.* 2011). Below the fluorescence linescan image are spatially averaged profiles (Fig. 4*B* and *C*) of the two areas indicated by the bars of corresponding colour on the image in Fig. 4*A*. The 'upper' region of the image had transients that maintained their maximally attained amplitudes throughout (while the baseline slowly increased). The transients in the more 'central' area of the image showed a decline in maximally attained amplitude that started at transient *l*. The broken lines above the spatially averaged profiles are included to help visual identification of the decline in the maximally attained amplitudes of the Ca^{2+} releases. Figure 4*D–R* shows each of the release fronts of the transients in Fig. 4*A* with an expanded time axis. Spatial inhomogeneity of

bars in *C* and *D*, respectively. Note that the longitudinally propagating APs are represented by a spatially averaged profile that has a very long rise time when averaged across the entire spatial dimension of the image but when the profile is restricted the rise time becomes much briefer and very similar to that observed following radially propagating APs.

the release front becomes obvious in Fig. 4*M* and this increases in Fig. 4 panels *N*–*R*. The increase in spatial inhomogeneity causes a delay in the spatially averaged Ca^{2+} release. The explanation for this behaviour may be different from that shown in Fig. 3 (see Discussion). The developing inhomogeneity observed in Fig. 4 was observed in two of three fibres stimulated at 10 Hz under the same conditions.

Propagation of tubular excitation across two dimensions of space

Next we examined the AP propagation with high speed confocal imaging of Ca^{2+} in *xyt* mode, with the slit scanning laser sweeping across the short axis of the fibre at 25 μs line^{-1}. This allowed the observation of AP propagation within the t-system across two dimensions of

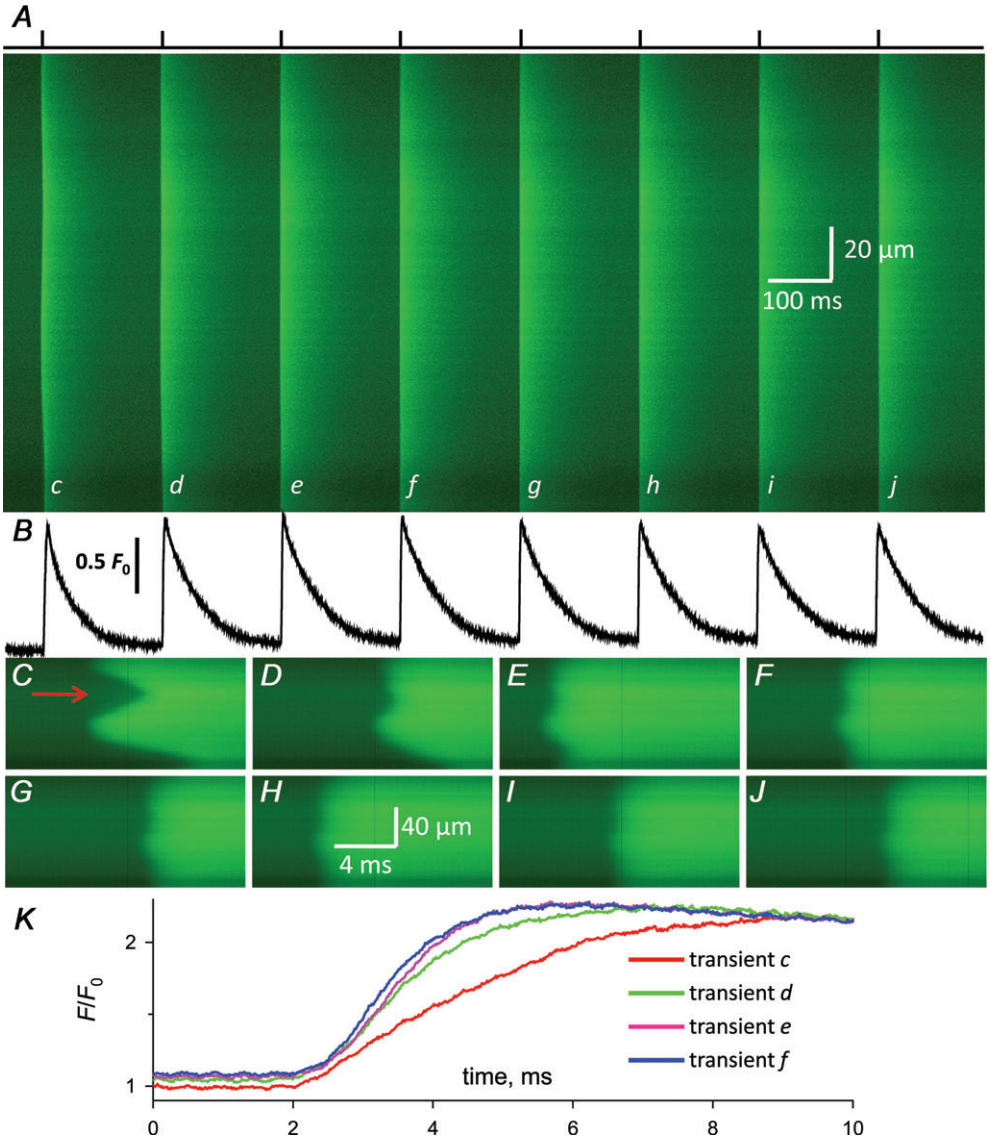

Figure 3. Longitudinally propagating APs in the t-system of fast-twitch fibres during EC coupling ensure a uniform release of Ca^{2+}
A, linescan image of OGB5N fluorescence from the cytoplasm of a skinned fibre in a region close to the longitudinal axis of the fibre during field stimulation at 5 Hz. The stimulation protocol is indicated at the top of the image and the spatially averaged profile is presented in *B*. Each Ca^{2+} transient is marked with a lower-case letter in *A* is displayed with an expanded time axis in the panel with the corresponding upper-case letter, *C*–*J*. Note that Ca^{2+} release was always continuous along the long axis of the fibre. The fronts of Ca^{2+} release at an angle to the scanning line indicate propagation of APs along longitudinal tubules into regions where transverse tubules initially failed to be excited by the field pulse. The amplitude and 10 to 90% rise time for each transient were, respectively: 1.18 and 4.19 ms (*c*); 1.23 and 3.35 ms (*d*); 1.27 and 2.43 ms (*e*); 1.26 and 2.12 ms (*f*); 1.20 and 2.31 ms (*g*); 1.20 and 3.02 ms (*h*); 1.17 and 3.13 ms (*i*); and 1.16 and 3.30 ms (*j*). *K*, spatially averaged profiles of transients *c*–*f* on an expanded time base.

space (longitudinal and transverse axes of the fibre) and time. Figure 5 shows selected $xy(t)$ images from a series where a skinned fibre bathed in an internal K^+-based solution with rhod-2 was stimulated by three successive field pulses that were about 0.5 s apart. The full *xyt* series is shown in the online Supplemental Material (Fig. S2). The first row of images shows the fibre responding uniformly along the long axis to field stimulation. The Ca^{2+} release

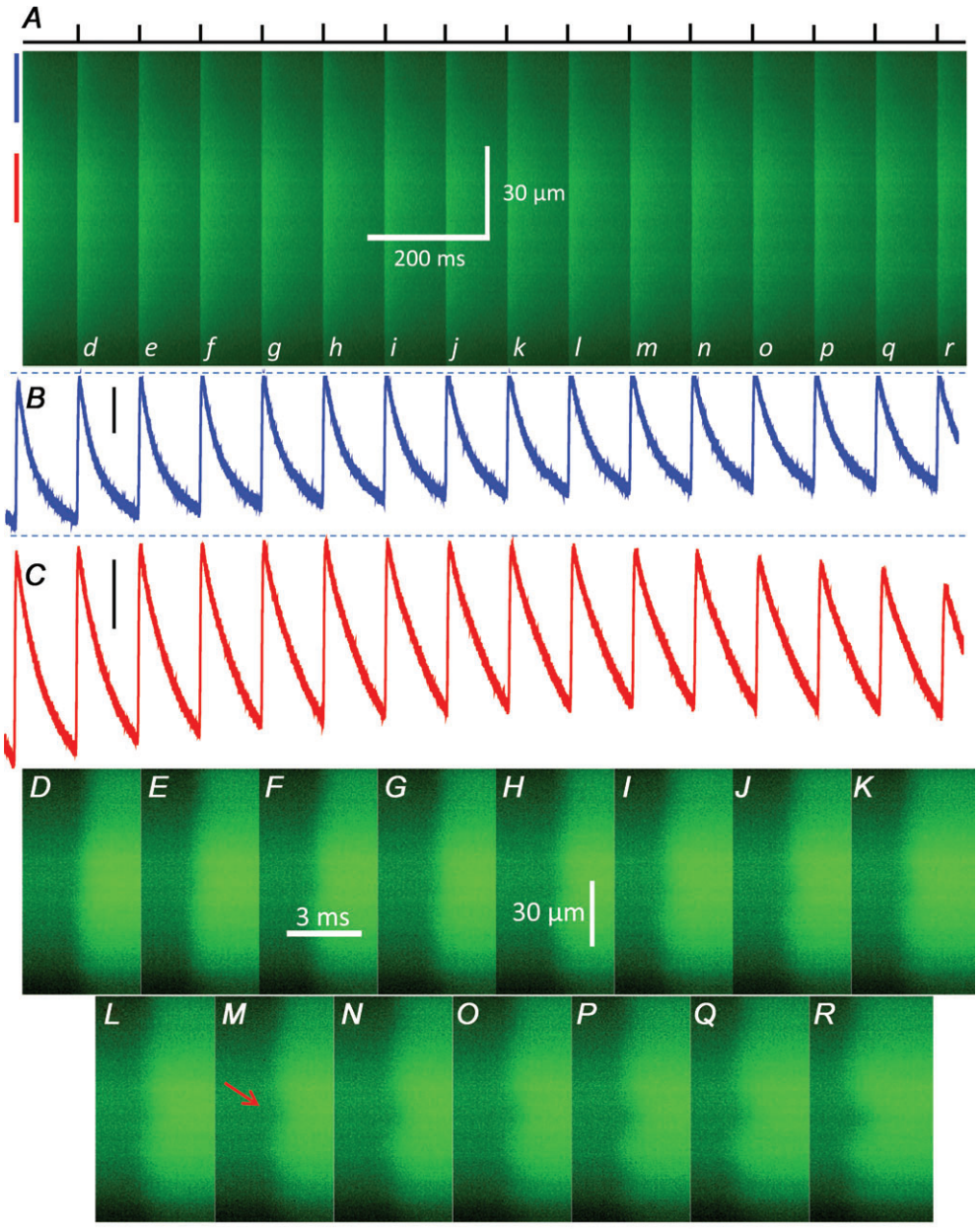

Figure 4. Local onset of high frequency fatigue in a fast-twitch fibre is offset by longitudinally propagating APs within the t-system
A, linescan image of OGB5N fluorescence from the cytoplasm of a skinned fibre in an area close to the longitudinal axis of the fibre during field stimulation at 10 Hz. The stimulation protocol is indicated at the top of the image and the spatially averaged profiles of the two regions indicated by the bars are presented below in corresponding colours in *B* and *C*. The vertical bars by each profile represent 0.2 F/F_0. Each Ca^{2+} transient is marked with a lower-case letter in *A* and is displayed on an expanded time axis in the panel with the corresponding upper-case letter, *D*–*R*. Note that the transients from the restricted spatially averaged profile from the top of the image shows consistent maximally attained amplitudes throughout whereas the profile from the middle of the image shows transients that decline in maximally attained amplitudes after transient *I*. The decline in amplitude of these transients is consistent with the delay in the rise of Ca^{2+} release in this region that has the same onset. The onset of a local delay in the action potential-induced Ca^{2+} release is indicated by the arrow in M.

is at its maximum in the first image taken following stimulation and then the cytoplasmic [Ca^{2+}] gradually declines. This is shown in profile at the end of the row of images in Fig. 5*A*, where the fluorescence intensity is spatially averaged over the time it takes to scan an image (12.6 ms) plus the time where there is no imaging, while the laser repositions itself for the next scan (20 ms). The images in Fig. 5*B* and *C* show different behaviour from that shown in Fig. 5*A*. In these instances only about half of the fibre was initially excited by the field pulse and released Ca^{2+}. In both cases, the '>' shape of the Ca^{2+} release pattern indicated that APs propagated into the areas where the transverse tubules failed to be initially excited by the field pulse. Deeper into the fibre the velocity of propagation was 8.8 μm ms^{-1}, the same as recorded in linescan mode across one dimension of space (Figs 2 and 3). However, the steeper angle also shown in the second panel of Fig. 5*B* (indicated by the red arrow) showed APs propagating at 26 μm ms^{-1} closer to the surface of the preparation. By the third frame of both *B* and *C*, Ca^{2+} release became more uniform, reached its maximum spatially averaged amplitude and then began to decline. The apparent uniformity of the third and fourth images in Fig. 5*B* and *C* compared with the respective second image in Fig. 5*A* is simply because of the fast rise and relatively slow decline of the Ca^{2+} transients. The direct consequence of a less uniform excitation along the fibre length is a markedly slower rate of rise of spatially averaged profiles as shown at the right of each row, indicating that the spatially averaged rise of the Ca^{2+} transient is considerably slowed when 15–20 adjacent sarcomeres of the ~50 imaged failed to be excited by the field pulse.

Note that failure of large numbers of adjacent transverse tubules to be excited by the field pulse indicates that the field pulse strength applied to the skinned fibre was not supramaximal for triggering action potentials simultaneously in the tubular network along the entire length of the fibre (Posterino *et al.* 2000; Stephenson, 2006). The '>' shape of Ca^{2+} release pattern also indicates the direction of AP propagation across the fibre (from left to right). The field pulse must trigger APs in the sealed t-system on one side of the preparation from where they propagate across the short axis of the fibre (Stephenson, 2006). This information on the direction of AP propagation allowed us to estimate the transverse velocity of AP propagation when fibres were uniformly excited along their long axis using two different methods. The first was to compare the Ca^{2+}-dependent fluorescence

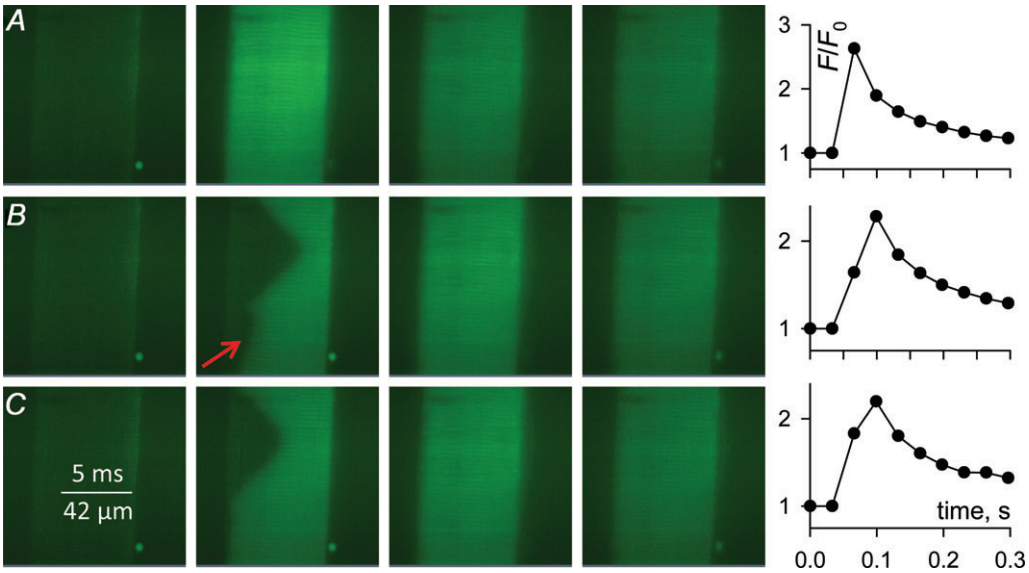

Figure 5. High speed confocal imaging of cytoplasmic Ca^{2+} in *xyt* mode during successive field stimuli shows constant rates of AP propagation across two dimensions of space
Selected cytoplasmic rhod-2 fluorescence images from a skinned fibre imaged in *xyt* mode at 25 μs line^{-1} during field stimulation. *A*, row of four sequential images that displayed a uniform release of Ca^{2+} upon field stimulation. The fluorescence profile is shown at right. *B* and *C*, rows of four sequentially collected images where the release of Ca^{2+} was not initially uniform across the fibre following field stimulation. Ca^{2+} release became uniform by the third frame as shown here, indicating the initially non-uniform excitation of the t-system network leads to APs propagating into these initially non-responding regions at 8.8 μm ms^{-1}. The red arrow indicates a region closer to the fibre surface where APs have propagated at 26 μm ms^{-1}. Fluorescence profiles are shown at the right. In all three examples the Ca^{2+} transients declined following the uniform release of Ca^{2+}. In the profiles, points 2–5 represent the images in each row (left-to-right), respectively. Note only the top profile reaches its maximum in the first frame following stimulation. Note there is a 20 ms gap between images as the laser repositions itself to scan again. The full *xyt* series is shown in the online Supplemental Material (Fig. S2).

signal across the short axis of the fibre with the scanning rate of the laser that sets the rate of signal acquisition. In the $xy(t)$ images at the top of Fig. 6 (the second and third panels of Fig. 5*A*) the rhod-2 fluorescence profile across the short axis of the fibre (parallel with the direction of scanning) indicated by the overlaid white trace of the images has a symmetrical, slightly convex shape. The convex shape may be created by dye binding to thicker sections of the preparation toward the fibre centre. From the symmetry of the fluorescence signal at equal distances from the fibre centre (along the fibre short axis) it follows that APs must have propagated across the fibre at a rate that must be close to the scanning speed of the laser at 8.4 μm ms^{-1}.

Another way of estimating the transverse velocity of AP propagation is by fitting the time delay required between the two dashed red lines drawn on each $xy(t)$ image at the top of Fig. 6 that represent linescans parallel to the long axis of the fibre to the requirement of very similar F/F_0 values for the entire duration of the Ca^{2+} transient across the *xy(t)* images (Fig. 6). The pairs of red lines in each *xy(t)* image shown in Fig. 6 are separated in time and space by 4.8 ms and 40 μm, respectively. Below the *xy(t)* images are two linescan profiles of rhod-2 fluorescence of a field stimulated skinned fibre separated by a delay of 4 ms. This delay between the linescans allows the drop-down arrows of the same length from the dashed red lines separated by 40 μm on the *xy(t)* images to meet the same F/F_0 values. Thus the APs must have propagated at a velocity close to 10 μm ms^{-1} between the dashed red lines to produce a fluorescence profile observed in the rapidly acquired $xy(t)$ images. We have fitted this model to linescans from three

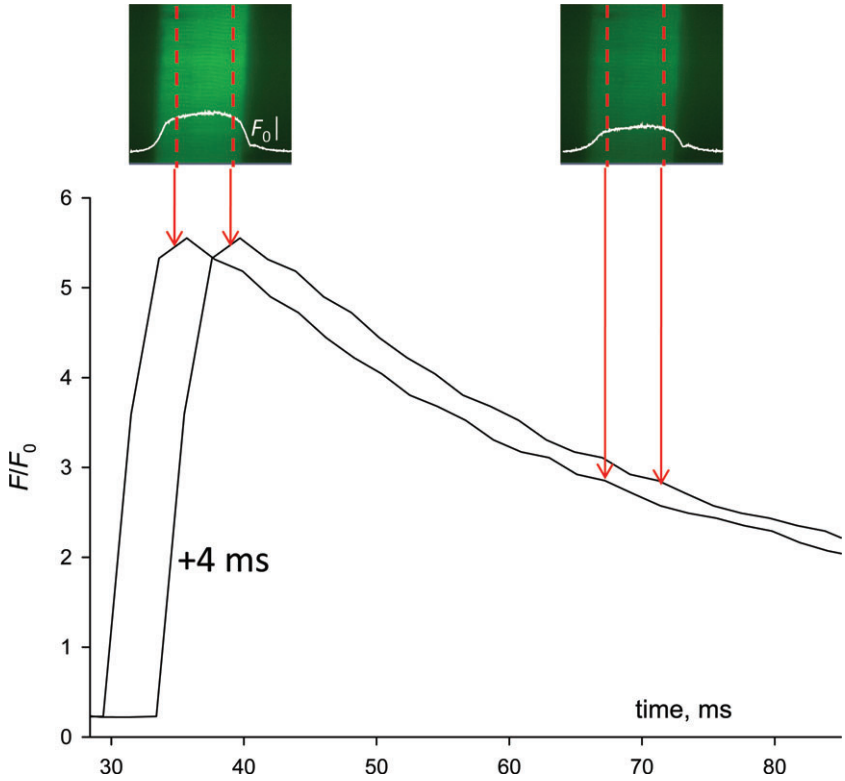

Figure 6. Estimation of the velocity of AP propagation across the short axis of the fibre
The spatially averaged profile from a confocal linescan of the cytoplasmic rhod-2 fluorescence signal imaged at 2.1 ms line^{-1} during field stimulation is shown. The original transient that starts closer to the origin is shifted in time by 4 ms to simulate how the fluorescence signal would evolve with such a delay. Note that during the declining phase of the fluorescence profiles there is a difference in F/F_0 in time. The fluorescence images at the top are the second and third panels from Fig. 5*A* that have been recorded in *xyt* mode at 25 μs line^{-1} with the scanning laser sweeping across the short axis of the fibre. These images therefore have a horizontal axis that is both time and space. The normalized fluorescence profile across the image is overlaid in white. The images are positioned above the linescan profiles aligned to the same time base. The two broken lines running vertically on each fluorescence image are used to indicate on the linescan profiles the time delay in transversal AP propagation that would be required to produce a uniform rhod-2 fluorescence signal in each *xy* image (i.e. drop arrows of same length, to same F/F_0 of the respective linescan profiles). The fit of the fluorescence signal in linescan profile and *xyt* mode requires that an AP would take 4 ms to propagate from the first to the second broken red line (40 μm) in each *xy* image, indicating a transversal propagation rate of 10 μm ms^{-1}.

other fibres to derive a radial propagation velocity of APs of 10.1 ± 0.7 μm ms^{-1}.

Pathways through the t-system network

The pathway along which action potentials move longitudinally inside the fibre can include the myofibrillar longitudinal tubules, realigning transverse tubules across misregistered sarcomeres and the subsarcolemmal t-system network (Launikonis & Stephenson, 2004; Edwards & Launikonis, 2008). In order to explain a faster longitudinal velocity of AP propagation close to the surface of the fibre than deeper into the fibre one would expect that more longitudinally connecting tubules would exist closer to the fibre surface than at the deeper layers to provide a shorter pathway for longitudinal AP propagation. In order to determine if this may be the case, mechanically skinned fibres with fluo-5N trapped in the t-system were imaged with a confocal microscope during successive steps through the axial plane of 1 μm. The image in Fig. 7*A* has the confocal plane positioned close to the periphery of a skinned fibre preparation. In this image transverse tubules where resolved in double rows under a mesh-work type pattern of tubules that appear to extend in all directions in agreement with previous studies (Murphy *et al.* 2009). These tubules represent the subsarcolemmal t-system network that links the sarcolemma to transverse tubules. This image also indicates that only the sarcolemma is removed from this preparation during mechanical skinning, leaving behind much of the subsarcolemmal, non-myofibrillar components of the fibre. At the next layer (Fig. 7*B*) many connections between the transverse tubules are evident and these become significantly less as the imaging plane is moved to more inner layers of the fibre (Fig. 7*C* and *D*). The deepest layer imaged (Fig. 7*D*) shows a low density of longitudinal tubules but also transverse tubules that realign across misregistered sarcomeres to provide further longitudinal connections along the long axis of the fibre that form the complex helicoidal structure originally described by Peachey & Eisenberg (1978). This progression of tubular structures was observed in all three fibres imaged in this manner.

To determine if the extent of longitudinally connecting tubules at each layer imaged was changing, we determined the proportion of pixels occupied by fluo-5N fluorescence that was trapped in the t-system for each distance from the fibre periphery. The fluo-5N fluorescence signals from the t-system were converted to binary images to allow a simple count of the area occupied by the t-system in each image. It was assumed that the proportion of pixels in each image occupied by the transverse tubules was the same within the border of the preparation. Any change in the proportion of pixels occupied by fluorescence was then due to the increase or decrease of longitudinally connecting tubules. Figure 8 shows that the proportion of pixels occupied by fluo-5N fluorescence (t-system area) decreased as the distance from the periphery of the preparation increased, indicating a reduction in the longitudinal connections deeper in the fibre.

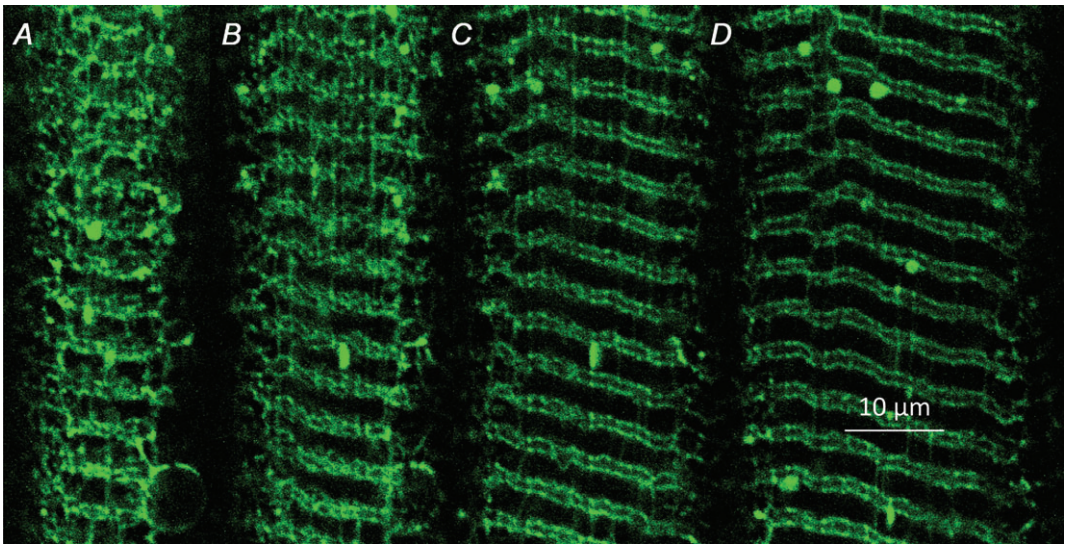

Figure 7. The t-system of fast-twitch rat EDL fibres displays more longitudinal connections closer to the surface of the fibre than at deeper planes
A–D, confocal images of fluo-5N fluorescence from the t-system of a skinned fibre. The image in *A* was an optical section taken closest to the periphery of the fibre. The subsequent images, *B* and *C*, are images taken from the same preparation following moving the confocal imaging plane toward the centre of the fibre at progressive steps of 1 μm.

Discussion

By imaging Ca^{2+} transients with high temporal resolution in fast-twitch mechanically skinned muscle fibres, where the sarcolemma is not present and the sealed tubular system is electrically excitable (Lamb & Stephenson, 1990; Posterino *et al.* 2000; Launikonis *et al.* 2006) (Figs 1–5), it was possible to trace the pathway of underlying APs through the t-system and determine the velocities of AP propagation of excitation in the t-system along the short and long axes of the fibre. Importantly, we show that APs move longitudinally and transversally through the t-system at similar velocities that are two orders of magnitude slower than the velocity of AP propagation along the sarcolemma of the muscle fibre. The difference in the velocities of AP propagation between the t-system and sarcolemma have important implications for the normal function of skeletal muscle and helps explain contractures in rippling muscle disease (RMD).

Transversal and longitudinal velocities of AP propagation in fast-twitch rat fibres

The vastly different cross-sectional area of the intact muscle fibre compared to that of the transverse tubules (Hodgkin, 1954) largely accounts for the different rates of action potential propagation across the respective membranes. At 22°C the conduction velocity of the sarcolemmal AP in EDL rat muscle has been estimated at $1\,m\,s^{-1}$ (Kössler *et al.* 1991). A factor of 35 is introduced to scale down the expected propagation velocity of the AP along the sarcolemma to that of the transverse tubules (proportional to the square root of their effective diameters; Hodgkin, 1954). With this correction the t-system AP velocity would be expected to be about $28\,\mu m\,ms^{-1}$ if otherwise the properties of the membranes were the same. This value is similar to that observed at the periphery of the t-system when the AP propagates longitudinally. Since the velocity of AP propagation is also dependent on other factors such as Na^+ channel density, this observation may indicate a similar Na^+ channel density in the sub-sarcolemmal t-system network and sarcolemma. The transversal propagation velocity of the AP in this study measured in a central region of the fibre was $10\,\mu m\,ms^{-1}$ (Figs 2, 5 and 6). Considering now that the transverse tubules wrap around each myofibril, the actual velocity of AP propagation along the transverse tubules must have been at least $15.7\,\mu m\,ms^{-1}$ to account for the t-system tortuosity (semicircle length/diameter $= \pi/2 = 1.57$). The lower density of Na^+ channels in the t-system deeper into the fibre than on the sarcolemma (Jaimovich *et al.* 1983) could then fully explain the reduced AP velocity in the transverse tubules in the central part of the fibre ($15.7\,\mu m\,ms^{-1}$ at 19°C) compared with an expected AP velocity of $22.8\,\mu m\,ms^{-1}$ at 19°C ($28\,\mu m\,ms^{-1}$ at 22°C assuming $Q_{10} = 2$; Kössler *et al.* 1991) when the measured AP velocity along the sarcolemma of rat EDL fibres ($1\,m\,s^{-1}$; Kössler *et al.* 1991) is corrected for differences in tortuosity and effective fibre/t-system diameters. From our results it appears that there is probably little difference in the conduction velocities along a longitudinally and transversally oriented tubule at certain distance from the fibre surface.

The relatively slow AP propagation within the t-system compared to that at the surface is sufficient to ensure the uniform excitation and release of Ca^{2+} in the rat fast-twitch fibre because of the short distances that the tubular APs need to travel. The entire surface of the fibre is excited within a matter of milliseconds as the AP spreads along the sarcolemma and enters the subsarcolemmal t-system network without delay, unlike the situation in the frog fibres (Woods *et al.* 2005). The subsequent slower inward propagation of excitation inside the fibre to the Ca^{2+} release units ensures that the sections of fibre closer to the neuromuscular junction do not release Ca^{2+} at any significant time before sections of fibre closer to the myotendinous junction. Thus this combination of a fast and slow spread of excitation along and within the fibre, respectively, is fundamental to a uniform release of Ca^{2+} through the fibre in a matter of milliseconds.

Furthermore if we adjust the rate for propagation of APs within the t-system for the difference between our experimental recording temperature and the physiological temperature in the mammalian body (37°C) using a Q_{10} of 2, we estimate the velocity to be $\sim 80\,\mu m\,ms^{-1}$. Therefore for a fibre of diameter 40 μm, radially propagating APs

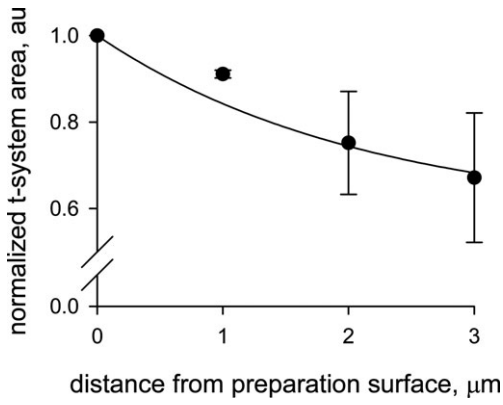

Figure 8. Longitudinally connecting elements of the t-system are denser closer to the fibre surface
The graph plots the proportion of fluo-5N fluorescence containing pixels within the border of the preparation as imaged at different depths from the fibre surface (see text). The image taken closest to the fibre surface (e.g. Fig. 7*A*) has been used as reference to normalize the images taken at distances further from the surface (e.g. Fig. 7*B–D*). The data obtained on three preparations have been fitted by an exponential curve.

from all points of the sarcolemma would excite the t-system in ∼0.25 ms. Note that the relatively small access resistance at the mouths of the t-tubules in mammalian fibres (Woods *et al.* 2005) would contribute little to the delay in the propagation of APs from the surface to the centre of the fibre and that the effective resistivity of the tubular network is expected to be the similar in our preparation to that in intact muscle considering that the volume of the tubular system in skinned rat fibres changes little compared with that in the intact fibre (Launikonis & Stephenson, 2002*a*, 2004).

APs in the t-system of healthy, fatigued and diseased muscles

Depolarization due to high frequency stimulation is most likely to be due to intracellular K^+ entering the t-system lumen during the repolarizing phase of closely spaced APs (Allen *et al.* 2008; Cairns & Lindinger, 2008) and has been shown to contribute to fatigue under physiological conditions (Cairns *et al.* 2011). The change in tubular $[K^+]$ has recently been modelled as being greatest at the innermost shells of the intact fibre (Fraser *et al.* 2011). This would slow the radial propagation of APs to the centre of the fibre. In skinned fibres there are not the same gradients along the transverse tubules as in intact fibres because the t-system is sealed. Our skinned fibre experiments have also been performed at temperatures significantly lower than physiological, which may affect ion conductances, diffusion and AP behaviour. However, we still observed such a 'fast onset fatigue' phenomenon, as have others (Dutka *et al.* 2008). In Fig. 4 we observed for the first time a local delay in the Ca^{2+} release front that developed progressively during a continuous train of supramaximal field pulses at 10 Hz. The non-uniform Ca^{2+} release front is most likely due to the progressive build-up of tubular $[K^+]$ in the area of the delayed onset of Ca^{2+} release, causing slow inactivation of Na^+ channels, increase in the threshold for AP generation and slower velocity of AP propagation. As the linescan was close to the centre of the fibre (diameter about 60 μm), the local delay developed in the Ca^{2+} release front could be explained if there was either a slowing of the transverse AP propagation by about 15% from the surface of the fibre, across this section of the fibre, or if APs propagating longitudinally from adjacent areas by-passed the region containing the tubules of reduced excitability.

A progressive build-up of tubular K^+ that depolarizes the t-system slowing excitation (Fig. 4) is different from the behaviour observed in Figs 3 and 5 where near-threshold field pulses resulted in combinations of uniform releases of Ca^{2+} and releases of Ca^{2+} that were spatially inhomogeneous to successive electrical pulses in no specific order. Because the examples in Figs 3 and 5 showed these combinations and not a developing delay in local Ca^{2+} release in response to repeated stimulation, the reason for this delay cannot be caused by tubular K^+ accumulation. The failure of some areas of the fibre to respond to field stimulation while others did respond indicates different AP thresholds in the transverse tubular networks along the length of the fibre. The continuous front of Ca^{2+} release into the areas that were not excited initially by the field pulse can only be explained by longitudinally propagating APs (Fig. 2; Posterino *et al.* 2000). This could be an important safety mechanism in situations where there is a chronic local depolarization of the t-system. Various situations such as t-system vacuolation or acute injury to a fibre may force the use of alternative excitation pathways through the t-system network to ensure uniform release of Ca^{2+} within the fibre and consequently uniform contraction. The t-system can vacuolate following fatiguing stimulation but the presence of such swellings does not affect force production during EC coupling (Lännergren *et al.* 1999) suggesting that Ca^{2+} release was not impaired. Vacuole formation during fatigue is associated with fluxes of water, Na^+, H^+ and lactate$^-$ (Lännergren *et al.* 2000; Hallerdei *et al.* 2010) that may cause local depolarization requiring the pathway of APs to some transverse tubules to be diverted through longitudinal tubules. However, the vacuolation of the t-system may also function as a safety mechanism to reduce the rise in luminal $[K^+]$ during fatiguing stimulation and also to increase the velocity of AP propagation in the t-system as a whole due to the marked increase in the t-system volume. Furthermore, when injuries to the t-system occur such as following bouts of eccentric contractions when transverse tubules can be severed from the sarcolemma the number of longitudinal tubules apparently increases (Takekura *et al.* 2001), which would facilitate the longitudinal propagation of APs to limit the loss of fibre function to the injured area.

Interesting observations in regards to the underlying mechanism of the rolling contractures that characterize RMD have been put forward by Lamb (2005). The proposal is based on the presence of longitudinally propagating APs through the t-system network that do not break-out to the surface of the fibre. Our study confirms that APs can propagate longitudinally solely within the t-system of muscle fibres to activate normal EC coupling (Fig. 2; Posterino *et al.* 2000). RMD is an autosomal-dominant disorder characterized by a mutation in the plasma membrane protein caveolin-3 with generally benign symptoms of hyperexcitability (Betz, 2001; Torbergsen, 2002). The contractures look like ripples along the muscle passing at a rate around 600 μm ms^{-1} along groups of fibres and activating adjacent ones (at body temperature; Ricker *et al.* 1989) but are silent in surface electromyography (EMG) (Vorgerd *et al.*

1999; Torbergsen, 2002). The absence of caveolin-3 may increase the sensitivity of the muscle to stretch (Sinha *et al.* 2011) to activate t-system APs that coordinate the release of Ca^{2+} to produce a local contracture. The spread of the rolling contracture is still faster than the velocity of t-system excitation propagation adjusted for body temperature ($\sim$80 μm ms^{-1}). This is, however, the conduction velocity along the t-system of a healthy muscle. In RMD patients and caveolin-3 null mice, the t-system becomes swollen or 'honeycomb-like' immediately under the sarcolemma and displays more longitudinal elements (Galbiati *et al.* 2001; Woodman *et al.* 2004). Dilatations of the t-system approaching 0.5 μm would increase t-system AP conduction velocity to that consistent with rolling contractures observed in RMD patients. The t-system APs will not excite the sarcolemma because of its higher access resistance. Consistent with a role for t-system APs, recent needle EMG measurements show low amplitude electrical activity during rolling contractures (Maki *et al.* 2011).

In summary, we have shown that APs propagate transversally and longitudinally through the t-system network of fast-twitch rat skeletal muscle fibres at about two orders of magnitude slower than across the surface of the fibre. The muscle may encounter a number of situations under which transverse tubules fail to be excited and require alternative pathways via the t-system network to ensure uniform excitability of the fibre as a whole. Furthermore, the ability of APs to propagate longitudinally within the t-system network of mammalian skeletal muscle probably underlies the rolling contractures observed in RMD.

References

Adrian RH, Costantin LL & Peachey LD (1969). Radial spread of contraction in frog muscle fibres. *J Physiol* **204**, 231–257.

Adrian RH & Peres A (1979). Charge movement and membrane capacity in frog muscle. *J Physiol* **289**, 83–97.

Allen DG, Lamb GD & Westerblad H (2008). Skeletal muscle fatigue: cellular mechanisms. *Physiol Rev* **88**, 287–232.

Baylor SM & Hollingworth S (2003). Sarcoplasmic reticulum calcium release compared in slow-twitch and fast-twitch fibres of mouse muscle. *J Physiol* **551**, 125–138.

Betz RC, Schoser BG, Kasper D, Ricker K, Ramírez A, Stein V, Torbergsen T, Lee YA, Nöthen MM, Wienker TF, Malin JP, Propping P, Reis A, Mortier W, Jentsch TJ, Vorgerd M & Kubisch C (2001). Mutations in CAV3 cause mechanical hyperirritability of skeletal muscle in rippling muscle disease. *Nat Genet* **28**, 218–219.

Calderón JC, Bolaños & Caputo C (2010). Myosin heavy chain isoforms composition and Ca^{2+} transients in fibres from enzymatically dissociated murine soleus and extensor digitorum longus muscles. *J Physiol* **588**, 267–279.

Cairns SP, Leader JP & Loiselle DS (2011). Exacerbated potassium-induced paralysis of mouse soleus muscle at 37°C *vis-à-vis* 25°C: implications for fatigue. *Pflugers Arch* **461**, 469–479.

Cairns SP & Lindinger MI (2008). Do multiple ionic interactions contribute to skeletal muscle fatigue? *J Physiol* **586**, 4039–4054.

Cheung A, Dantzig JA, Hollingworth S, Baylor SM, Goldman YE, Mitchison TJ & Straight AF (2002). A small-molecule inhibitor of skeletal muscle myosin II. *Nat Cell Biol* **4**, 83–88.

Drummond GB (2009). Reporting ethical matters in *The Journal of Physiology*: standards and advice. *J Physiol* **587**, 713–719.

Dulhunty AF (1979). Distribution of potassium and chloride permeability over the surface and T-tubule membranes of mammalian skeletal muscle. *J Membr Biol* **45**, 293–310.

Dulhunty AF, Gage PW & Lamb GD (1986). Differential effects of thyroid hormone on T-tubules and terminal cisternae in rat muscles: an electrophysiological and morphometric analysis. *J Muscle Res Cell Motil* **7**, 225–236.

Dutka TL, Murphy RM, Stephenson DG & Lamb GD (2008). Chloride conductance in the transverse tubular system of rat skeletal muscle fibres: importance in excitation–contraction coupling and fatigue. *J Physiol* **586**, 875–887.

Edwards JN & Launikonis BS (2008). The accessibility and interconnectivity of the tubular system network in toad skeletal muscle. *J Physiol* **586**, 5077–5089.

Edwards JN, Macdonald WA, van der Poel C & Stephenson DG (2007). $O_2^{\bullet-}$ production at 37°C plays a critical role in depressing tetanic force of isolated rat and mouse skeletal muscle. *Am J Physiol Cell Physiol* **293**, C650–C660.

Eisenberg BR (1983). Quantitative ultrastructure of mammalian skeletal muscle. In *Handbook of Physiology*, section 10, *Skeletal Muscle*, ed. Peachey LD, pp. 73–112. American Physiological Society, Bethesda, MD, USA.

Endo M, Tanaka M & Ogawa Y (1970). Calcium induced calcium release from the sarcoplasmic reticulum of skinned skeletal muscle fibres. *Nature* **228**, 34–36.

Ford LE & Podolsky RJ (1970). Regenerative calcium release within muscle cells. *Science* **167**, 58–59.

Fraser JA, Huang CLH & Pedersen TH (2011). Relationships between resting conductances, excitability, and t-system ionic homeostasis in skeletal muscle. *J Gen Physiol* **138**, 95–116.

Galbiati F, Engelman JA, Volonte D, Zhang XL, Minetti C, Li M, Hou H Jr, Kneitz B, Edelmann W & Lisanti MP (2001). Caveolin-3 null mice show a loss of caveolae, changes in the microdomain distribution of the dystrophin-glycoprotein complex, and t-tubule abnormalities. *J Biol Chem* **276**, 21425–21433.

Gonzalez-Serratos H (1971). Inward spread of activation in vertebrate muscle fibres. *J Physiol* **212**, 777–799.

Jaimovich E, Chicheportiche R, Lombet A, Lazdunski M, Ildefonse M & Rougier O (1983). Differences in the properties of Na channels in muscle surface and T-tubular membranes revealed by tetrodotoxin derivatives. *Pflugers Arch* **397**, 1–5.

Julian FJ, Rome LC, Stephenson DG & Striz S (1986). The influence of free calcium on the maximum speed of shortening in skinned frog muscle fibres. *J Physiol* **380**, 257–273.

Hallerdei J, Scheibe RJ, Parkkila S, Waheed A, Sly WS, Gros G, Wetzel P & Endeward V (2010). T tubules and surface membranes provide equally effective pathways of carbonic anhydrase-facilitated lactic acid transport in skeletal muscle. *PLoS ONE* **5**, e15137.

Hodgkin AL (1954). A note on conduction velocity. *J Physiol* **125**, 221–224.

Hodgkin AL & Nakajima S (1972). Analysis of the membrane capacity in frog muscle. *J Physiol* **221**, 121–136.

Kössler F, Lange F, Caffier G & Küchler G (1991). External potassium and action potential propagation in rat fast and slow twitch muscles. *Gen Physiol Biophys* **10**, 485–498.

Lamb GD (2005). Rippling muscle disease may be caused by 'silent' action potentials in the tubular system of skeletal muscle fibers. *Muscle Nerve* **31**, 652–658.

Lamb GD & Stephenson DG (1990). Calcium release in skinned fibres of the toad by transverse tubule depolarization or by direct stimulation. *J Physiol* **423**, 495–517.

Lamb GD & Stephenson DG (1994). Effects of intracellular pH and [Mg^{2+}] on excitation–contraction coupling in skeletal muscle fibres of the rat. *J Physiol* **478**, 331–339.

Lännergren J, Bruton JD & Westerblad H (1999). Vacuole formation in fatigued single muscle fibres from frog and mouse. *J Muscle Res Cell Motil* **20**, 19–32.

Lännergren J, Bruton JD & Westerblad H (2000). Vacuole formation in fatigued skeletal muscle fibres from frog and mouse: effects of extracellular lactate. *J Physiol* **526**, 597–611.

Launikonis BS & Stephenson DG (2000). Effects of Mg^{2+} on Ca^{2+} release from sarcoplasmic reticulum of skeletal muscle fibres from yabby (crustacean) and rat. *J Physiol* **526**, 299–312.

Launikonis BS & Stephenson DG (2002*a*). Tubular system volume changes in twitch fibres from toad and rat skeletal muscle assessed by confocal microscopy. *J Physiol* **538**, 607–618.

Launikonis BS & Stephenson DG (2002*b*). Properties of the vertebrate skeletal muscle tubular system as a sealed compartment. *Cell Biol Int* **26**, 921–929.

Launikonis BS & Stephenson DG (2004). Osmotic properties of the sealed tubular system of toad and rat skeletal muscle. *J Gen Physiol* **123**, 231–247.

Launikonis BS, Zhou J, Royer L, Shannon TR, Brum G & Ríos E (2006). Depletion 'skraps' and dynamic buffering inside the cellular Ca^{2+} store. *Proc Natl Acad Sci U S A* **103**, 2982–2987.

Macdonald WA, Pedersen TH, Clausen T & Neilsen OB (2005). *N*-Benzyl-*p*-toluene sulphonomide allows the recording of trains of intracellular action potentials from nerve stimulated intact fast-twitch skeletal muscle of the rat. *Exp Physiol* **90**, 815–825.

Maki T, Matsumoto R, Kohara N, Kondo T, Son I, Mezaki T, Nishino I, Ikeda A & Takahashi R (2011). Rippling is not always electrically silent in Rippling muscle disease. *Muscle Nerve* **43**, 601–605.

Murphy RM, Mollica J & Lamb GD (2009). Plasma membrane removal in rat skeletal muscle fibers reveals caveolin-3 hot-spots at the neck of transverse tubules. *Exp Cell Res* **315**, 1015–1028.

Nakajima S & Gilai A (1980). Radial propagation of muscle action potential along the tubular system examined by potential-sensitive dyes. *J Gen Physiol* **76**, 751–762.

Ørtenblad N & Stephenson DG (2003). A novel signalling pathway originating in mitochondria modulates rat skeletal muscle membrane excitability. *J Physiol* **548**, 139–145.

Peachey LD & Eisenberg BR (1978). Helicoids in the T system and striations of frog skeletal muscle fibres seen by high voltage electron microscopy. *Biophys J* **22**, 145–154.

Posterino GS & Lamb GD (2003). Effect of sarcoplasmic reticulum Ca^{2+} content on action potential-induced Ca^{2+} release in rat skeletal muscle fibres. *J Physiol* **551**, 219–237.

Posterino GS, Lamb GD & Stephenson DG (2000). Twitch and tetanic force responses and longitudinal propagation of action potentials in skinned skeletal muscle fibres of the rat. *J Physiol* **527**, 131–137.

Quiñonez M, González F, Morgado-Valle C & DiFranco M (2010). Effects of membrane depolarization and changes in extracellular [K^+] on the Ca^{2+} transients of fast skeletal muscle fibers. Implication for muscle fatigue. *J Muscle Res Cell Mot* **31**, 13–33.

Ricker K, Morley RT & Rohkamm R (1989). Rippling muscle disease. *Arch Neurol* **46**, 405–408.

Rome LC (2006). Design and function of superfast muscles: new insights into physiology of skeletal muscle. *Annu Rev Physiol* **68**, 193–221.

Shirokova N, García J, Pizarro G & Ríos E (1996). Ca^{2+} release from the sarcoplasmic reticulum compared in amphibian and mammalian skeletal muscle. *J Gen Physiol* **107**, 1–18.

Sinha B, Köster D, Ruez R, Gonnord P, Bastiani M, Abankwa D, Stan RV, Butler-Browne G, Vedie B, Johannes L, Morone N, Parton RG, Raposo G, Sens P, Lamaze C & Nassoy P (2011). Cells respond to mechanical stress by rapid disassembly of caveolae. *Cell* **144**, 402–413.

Stephenson DG (2006). Tubular system excitability: an essential component of excitation-contraction coupling in fast-twitch fibres of vertebrate skeletal muscle. *J Muscle Res Cell Mot* **27**, 259–274.

Takekura H, Fujinami N, Nishizawa T, Ogasawara H & Kasuga N (2001). Eccentric exercise-induced morphological changes in the membrane systems involved in excitation–contraction coupling in rat skeletal muscle. *J Physiol* **553**, 571–583.

Torbergsen T (2002). Rippling muscle disease: a review. *Muscle Nerve* **11**, S103–S107.

Veratti E (1961). Investigations on the fine structure of striated muscle fiber. *J Biophys Biochem Cytol* **10**, 1–59.

Vorgerd M, Bolz H, Patzold T, Kubisch C, Malin J-P & Mortier W (1999). Phenotypic variability in rippling muscle disease. *Neurology* **52**, 1453–1459.

Woodman SE, Sotgia F, Galbiati F, Minetti C & Lisanti MP (2004). Caveolinopathies: mutations in caveolin-3 cause four distinct autosomal dominant muscle diseases. *Neurology* **62**, 538–543.

Woods CE, Novo D, DiFranco M, Capote J & Vergara JL (2005). Propagation in the transverse tubular system and voltage dependence of calcium release in normal and *mdx* mouse muscle fibres. *J Physiol* **568**, 867–880.

Young IS & Rome LC (2001). Mutually exclusive muscle designs: the power output of the locomotory and sonic muscles of the oyster toadfish (*Opsanus tau*). *Proc Biol Sci* **268**, 1965–1970.

Zhou J, Brum G, González A, Launikonis BS, Stern MD & Ríos E (2005). Concerted *vs*. sequential. Two activation patterns of vast arrays of intracellular Ca^{2+} channels in muscle. *J Gen Physiol* **126**, 301–309.

Author contributions

All authors approved the final version of this paper for publication. All experiments were performed at The University of Queensland. J.N.E. and B.S.L designed the experiments; J.N.E. and T.R.C. performed the experiments; J.N.E., B.S.L., D.G.S. and T.R.S. analysed data; B.S.L. and D.G.S. wrote the paper.

Acknowledgements

We thank Diane Muller (Zeiss) and Luke Hammond (University of Queensland) for organizing our access to the Zeiss 5 LIVE for these experiments. This work was supported by an Australian Research Council Discovery Project to B.S.L. and D.G.S.; the Leonie Stanley Memorial Fund of Muscular Dystrophy Queensland (Australia) to B.S.L.; and a University of Queensland Travel Award to T.R.S. and B.S.L. J.N.E. was a C.J. Martin Fellow of the National Health & Medical Research Council (Australia).

Author's present address

J. N. Edwards: Department of Molecular Biophysics and Physiology, Rush University Medical Centre, Chicago, IL, USA.